PAPER • OPEN ACCESS

Spider web-structured labyrinthine acoustic metamaterials for low-frequency sound control

New Journal of Physics
The open access journal at the forefront of physics

Deutsche Physikalische Gesellschaft DPG
IOP Institute of Physics

Published in partnership with: Deutsche Physikalische Gesellschaft and the Institute of Physics

OPEN ACCESS

RECEIVED
28 December 2016

REVISED
9 June 2017

ACCEPTED FOR PUBLICATION
3 August 2017

PUBLISHED
3 October 2017

PAPER

Spider web-structured labyrinthine acoustic metamaterials for low-frequency sound control

A O Krushynska[1,6], F Bosia[1], M Miniaci[2] and N M Pugno[3,4,5,6]

[1] Department of Physics and Nanostructured Interfaces and Surfaces Inter-departmental Centre, University of Torino, Via Pietro Giuria 1, I-10125 Torino, Italy
[2] University of Le Havre, Laboratoire Ondes et Milieux Complexes, UMR CNRS 6294, 75 Rue Bellot, F-76600 Le Havre, France
[3] Laboratory of Bio-Inspired and Graphene Nanomechanics, Department of Civil, Environmental and Mechanical Engineering, University of Trento, Via Mesiano 77, I-38123 Trento, Italy
[4] School of Engineering and Materials Science, Queen Mary University of London, Mile End Road, London E1 4NS, United Kingdom
[5] Ket Lab, Edoardo Amaldi Foundation, Italian Space Agency, Via del Politecnico snc, I-00133 Rome, Italy
[6] Authors to whom any correspondence should be addressed.

E-mail: akrushynska@unito.it **and** nicola.pugno@unitn.it

Keywords: acoustic metamaterials, labyrinthine metamaterials, negative refraction, effective refractive index, bioinspired structures, finite element method

Abstract

Attenuating low-frequency sound remains a challenge, despite many advances in this field. Recently-developed acoustic metamaterials are characterized by unusual wave manipulation abilities that make them ideal candidates for efficient subwavelength sound control. In particular, labyrinthine acoustic metamaterials exhibit extremely high wave reflectivity, conical dispersion, and multiple artificial resonant modes originating from the specifically-designed topological architectures. These features enable broadband sound attenuation, negative refraction, acoustic cloaking and other peculiar effects. However, hybrid and/or tunable metamaterial performance implying enhanced wave reflection and simultaneous presence of conical dispersion at desired frequencies has not been reported so far. In this paper, we propose a new type of labyrinthine acoustic metamaterials (LAMMs) with hybrid dispersion characteristics by exploiting spider web-structured configurations. The developed design approach consists in adding a square surrounding frame to sectorial circular-shaped labyrinthine channels described in previous publications (e.g. (11)). Despite its simplicity, this approach provides tunability in the metamaterial functionality, such as the activation/elimination of subwavelength band gaps and negative group-velocity modes by increasing/decreasing the edge cavity dimensions. Since these cavities can be treated as extensions of variable-width internal channels, it becomes possible to exploit geometrical features, such as channel width, to shift the band gap position and size to desired frequencies. Time transient simulations demonstrate the effectiveness of the proposed metastructures for wave manipulation in terms of transmission or reflection coefficients, amplitude attenuation and time delay at subwavelength frequencies. The obtained results can be important for practical applications of LAMMs such as lightweight acoustic barriers with enhanced broadband wave-reflecting performances.

1. Introduction

Manipulating low-frequency sound remains a challenging task for scientists and engineers, despite a vast amount of research in the field. Efficient shielding of sound by means of conventional or artificial materials with low refractive indexes requires the construction of impractically thick and/or heavy structures that are not economically sustainable [1]. Recently developed acoustic metamaterials offer a new approach for manipulating low-frequency sound thanks to the extraordinary functionality originating from their structure rather than from

the constituents. Acoustic metamaterials are engineered composites with unusual effective characteristics, e.g. negative bulk modulus and/or mass density, zero or negative effective refractive index, etc. These metamaterials can formally be divided into locally resonant metamaterials with basic units incorporating resonators [2, 3] and other metastructures described by effective medium theories [4–6]. The latter comprise so-called 'labyrinthine' or 'space-coiling' metamaterials with a geometry-based mechanism for controlling subwavelength acoustic waves [7–11].

The advanced functionalities provided by labyrinthine acoustic metamaterials (LAMMs) are based on the creation of a network of subwavelength internal channels (labyrinths) in non-resonant unit cells in order to extend wave propagation paths. This results in a substantial reduction of the effective propagation velocity with respect to a homogeneous medium. Also, physical models of labyrinthine unit cells in the subwavelength scale can be characterized as layered structures with effective material parameters having extreme values, such as unusually high effective refractive indexes and 'double negativity' (i.e. simultaneous negativity of the effective density and bulk modulus) [7, 8, 10, 11]. The space-coiling approach opens a simple and reliable way for designing versatile, easy-to-fabricate acoustic metamaterials with isotropic response, which are capable of controlling sound waves at low, deep subwavelength frequencies [8]. This is a particularly desirable characteristic when long-wavelength phenomena need to be addressed, e.g. in the case of large-scale mechanical metamaterials for seismic shielding [12].

The theoretical concept of labyrinthine metamaterials was first proposed by Liang and Li [7] by analyzing configurations with folded zig-zag channels rotated relative to each other, to achieve isotropic performance. Later, their extreme and unique effective characteristics, such as negative refraction and near-zero or extremely positive/negative mass density, were demonstrated experimentally for acoustic [8–10] and electromagnetic [8] waves at kHz and GHz frequencies. The dispersion spectra of this type of LAMMs are characterized by a conical structure formed by almost straight bands with infinitesimal gaps between them, ensuring negligible effective dispersion and almost uniform wave transmission in wide frequency ranges [7, 8, 10]. Note that high values of the effective refractive index result in poor impedance matching for LAMMs with air, which can be improved by employing tapered channels and apertures in the unit cell design [13].

The ability of labyrinthine structures to scatter waves at a subwavelength scales can be significantly increased by exploiting artificial spatial concentration of sound in Mie-type resonant modes [11, 14]. This was first demonstrated by developing ultra-sparse highly-reflecting acoustic absorbers with sectorial circular channels allowing advanced reflection of low-frequency airborne sound [11]. In terms of dispersion properties, the presence of the artificial resonances results in opening subwavelength band gaps. However, conical dispersion and bands with negative group velocity disappear as the distance between the unit cells increases.

In this paper, we propose a new type of LAMMs with *hybrid* dispersion properties characterized by simultaneous subwavelength band gaps *and* negative group-velocity modes. The hybridization is achieved by adding a surrounding square frame to the LAMM configuration with sectorial circular-shaped channels [11]. From the structural point of view, this simple modification results in the creation of air cavities at the unit cell edges, which can be also considered as extensions of the curved channels, resulting in a variable channel width. In terms of metamaterial functionality, several non-trivial advantages appear, such as tunable dispersion properties and enhanced wave reflection within the band gap frequencies.

We demonstrate that the added edge cavities (or variability in the channel width) significantly influence the wave propagation characteristics of the designed LAMMs and enable to switch on/off subwavelength band gaps simply by varying the cavity size, while other geometric parameters are unchanged. Such a tunability can be important for engineering applications, especially when there are restrictions on the structural sizes. Moreover, we propose to exploit periodic and non-periodic variations in the channel width as a means for achieving desired wave control, i.e. for tuning the band gap and negative group-velocity modes to required frequency ranges. The corresponding analysis of the related effects is presented in detail. The developed structures can easily be manufactured by means of additive manufacturing techniques or computer-aided automated machining, similarly to any other LAMMs [10, 11, 13].

Since both the overall structure of the developed metamaterials (figure 1) and also the types of introduced non-uniformities are reminiscent of the geometry of spider webs, typically consisting of a bearing frame and two circumferential parts separated by an air cavity [15–17], we choose to indicate the proposed LAMM as 'spider web-structured'. Clearly, with this term we do not imply that spider webs are capable of manipulating sound waves [18], although recent application of spider web-inspired geometries for designing locally-resonant acoustic metamaterials has revealed several advantages in terms of low-frequency elastic wave manipulation [19].

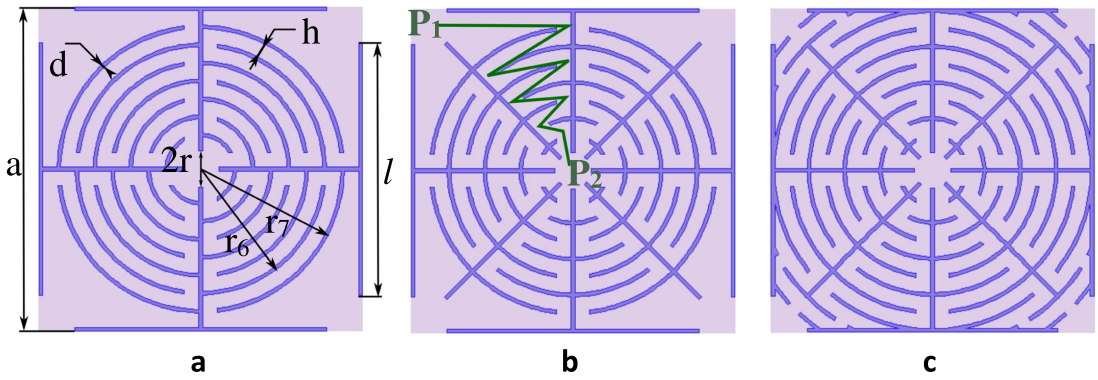

Figure 1. Unit cells of spider web-structured LAMMs comprising four (a) and eight (b), (c) curved channels connected at the unit cell center. In unit cell (c) (referred to as a spider web-structured LAMM with filled cavities) the curved channels extend to completely fill the edge cavities. Solid aluminum walls are represented in blue, air in violet. The unit cell geometry is determined by 7 parameters indicated in (a). Within a unit cell, sound waves propagate from point P1 to point P2 along the curved path indicated in (b) by the green line.

2. Model and methods

2.1. LAMM structure

The LAMM configurations consist of a square external frame and a circular 'labyrinth' divided into either four or eight independent circular-shaped channels connected at the center. Schematic diagrams in figures 1(a), (b) show the unit-cell cross sections with thin elements indicating solid walls (depicted in blue) surrounded by air (in violet).

Form a structural point of view, the designed configurations differ from those described in [11] only in the presence of a surrounding frame or, equivalently, in the presence of edge cavities, which can also be considered as non-uniform extensions of the internal curved channels. This simple distinction significantly influences the wave manipulation performance of the metamaterial, as demonstrated below. In particular, the introduced variable geometrical features affect the subwavelength wave dispersion, which results in hybrid and tunable responses.

In order to confirm the hybrid wave manipulation performance, we also consider configurations with edge cavities completely filled by extended curved channels, i.e. with the size of edge cavities tending to zero, which we refer to as 'spider web-structured LAMMs with filled cavities'. An example of the corresponding unit cell with 8 curved channels is shown figure 1(c).

Spider-web structured LAMM geometries can be defined by seven parameters: the lattice constant a; the thickness of solid walls d; the length of side walls l; the radius of the internal cavity r; the width of a passage between channels h, the curling number N (or the number of circles used to create the curved channels) and the external radius r_i ($i = 1, \ldots, N$) of curved walls (these parameters are indicated in figure 1(a)). We consider $a = 0.9$ m, $d = 0.01$ m, $l = 0.73$ m, $r = 0.05$ m, $h = 0.05$ m, $N = 7$, $r_i = 0.05 \cdot (i + 1)$, $i = 1, \ldots, 7$. The walls are made of aluminum with Young's modulus $E = 70$ GPa, Poisson's ratio $\nu = 0.33$, and mass density $\rho = 2700$ kg m^{-3}. Standard values for air, i.e. mass density $\rho = 1.225$ kg m^{-3}, atmospheric pressure of 10^5 Pa, and speed of sound $c = 343$ m s^{-1}, are used.

In terms of geometrical acoustics representation, sound waves propagate within the unit cells along the curved channels as indicated by the thick solid line in figure 1(b) instead of along the straight dashed line linking the external point P_1 to the unit cell center P_2. As a result, the wave path is increased by a factor of approximately 4 and 2.4 for four and eight-channel unit cells, respectively. This factor is known as coiling coefficient η and is evaluated as the ratio between the total length of the path and the unit cell pitch [13]. For the eight- and four-channel unit cells with edge cavities, the coiling coefficient equals to $\eta^{(8)} = 3.4$ and $\eta^{(4)} = 5.5$, respectively. A rough estimation of the metamaterial refractive index as a function of frequency can then be obtained as $n_{\text{eff}} = \eta - 2\pi c/\omega a$ [9].

2.2. Calculation of dispersion spectra

Dispersion properties of the spider web-structured LAMMs are numerically evaluated by means of finite-element simulations using the Pressure Acoustics module of COMSOL Multiphysics. We consider propagation of plane pressure waves $p = p_0(\boldsymbol{x})e^{i\omega t}$ of angular frequency ω governed by the Helmholtz equation:

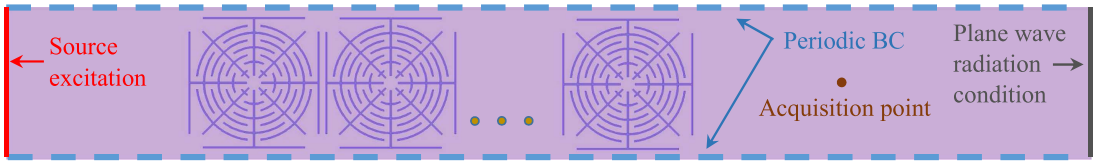

Figure 2. Model for transient analysis of sound waves propagating thought a set of labyrinthine metamaterial unit cells. A Gaussian modulated sinusoidal pulse is excited on the left boundary, and the transmitted signal is recorded at the acquisition point. Periodic boundary conditions reproduce an infinite medium in the vertical direction, while a plane wave radiation condition eliminates signal reflections from the right boundary.

$$\nabla \cdot \left(-\frac{1}{\rho_0}\nabla p_0\right) - \frac{\omega^2}{\rho_0 c^2} p_0 = 0 \tag{1}$$

in an infinite periodic LAMM medium with the Floquet–Bloch periodic conditions at the unit cell boundaries:

$$p_0(\boldsymbol{x} + a) = p_0(\boldsymbol{x})\mathrm{e}^{-ka}. \tag{2}$$

Given the large unit cell length $a = 0.9$ m and rather small curling number $N = 7$, the sound pressure field may be regarded as lossless in the sense that thermo-viscous boundary layers accompanying wave propagation can be neglected [8, 11]. At the solid walls, we prescribe sound-hard boundary conditions that imply vanishing normal sound velocity, i.e. $\partial p_0/\partial n = 0$, where n indicates an external normal to a wall. This is justified by an impedance value of aluminum four orders larger than that of air, as has been experimentally verified [10].

2.3. Transmission analysis

The ability of the proposed LAMMs to block the propagation of low-frequency acoustic waves can be confirmed by analyzing their transmission characteristics. In particular, we examine plane pressure waves propagating along the horizontal direction (Γ–X) through a varying number of closely located unit cells (the center-to-center distance between unit cells is a). The simulations are performed in the frequency domain using COMSOL Multiphysics.

2.4. Transient analysis

To estimate wave manipulation capabilities of the developed LAMMs at low frequencies, we numerically simulate a time-dependant pulse propagation through a set of metamaterial unit cells and evaluate the amount of transmitted and reflected wave energy. The analysis is performed for the eight-channel spider web-structured unit cells and those without external frames.

The time-dependent acoustic pressure field $p(\boldsymbol{x}, t)$ is governed by the scalar wave equation:

$$\nabla \cdot \left(-\frac{1}{\rho}\nabla p\right) + \frac{1}{\rho c^2}\frac{\partial^2 p}{\partial t^2} = S(t). \tag{3}$$

Source waves are unity-amplitude Gaussian modulated sinusoidal pulses of in the form of

$$S(t) = \sin(2\pi f_c t)\exp(-t^2/2\sigma^2) \tag{4}$$

with f_c denoting the carrier frequency, σ the standard deviation of the Gaussian pulse, and $2\pi\sigma$ the pulse width.

The model is shown in figure 2 and consists of closely-located unit cells (or a single unit cell) at a center-to-center distance a. At the top and bottom domain boundaries, periodic continuity conditions are applied to simulate an infinite medium in the vertical direction. On the right boundary, a plane wave radiation condition is used in order to minimize spurious reflections from normally incident waves. Uniformly distributed pressure variations (equation (4)) are applied on the left boundary to simulate plane acoustic waves, such as those launched by a loudspeaker located at a large distance from the metamaterial region (e.g. as in the experiments reported in [10]). The acquisition point is chosen at a distance a on the right side from the unit cells. The simulations are numerically performed by means of COMSOL Multiphysics neglecting any losses due to the chosen sizes of the metastructures [11].

3. Results

3.1. Dispersion characteristics

Figure 3(a) shows a dispersion diagram for a spider web-structured unit cell with eight sectorial channels. The horizontal axis indicates the values of wave vector $\boldsymbol{k}$ along the borders (Γ–X–M) of the triangular irreducible Brillouin zone for a square periodic lattice [20], while the vertical axis shows normalized frequencies,

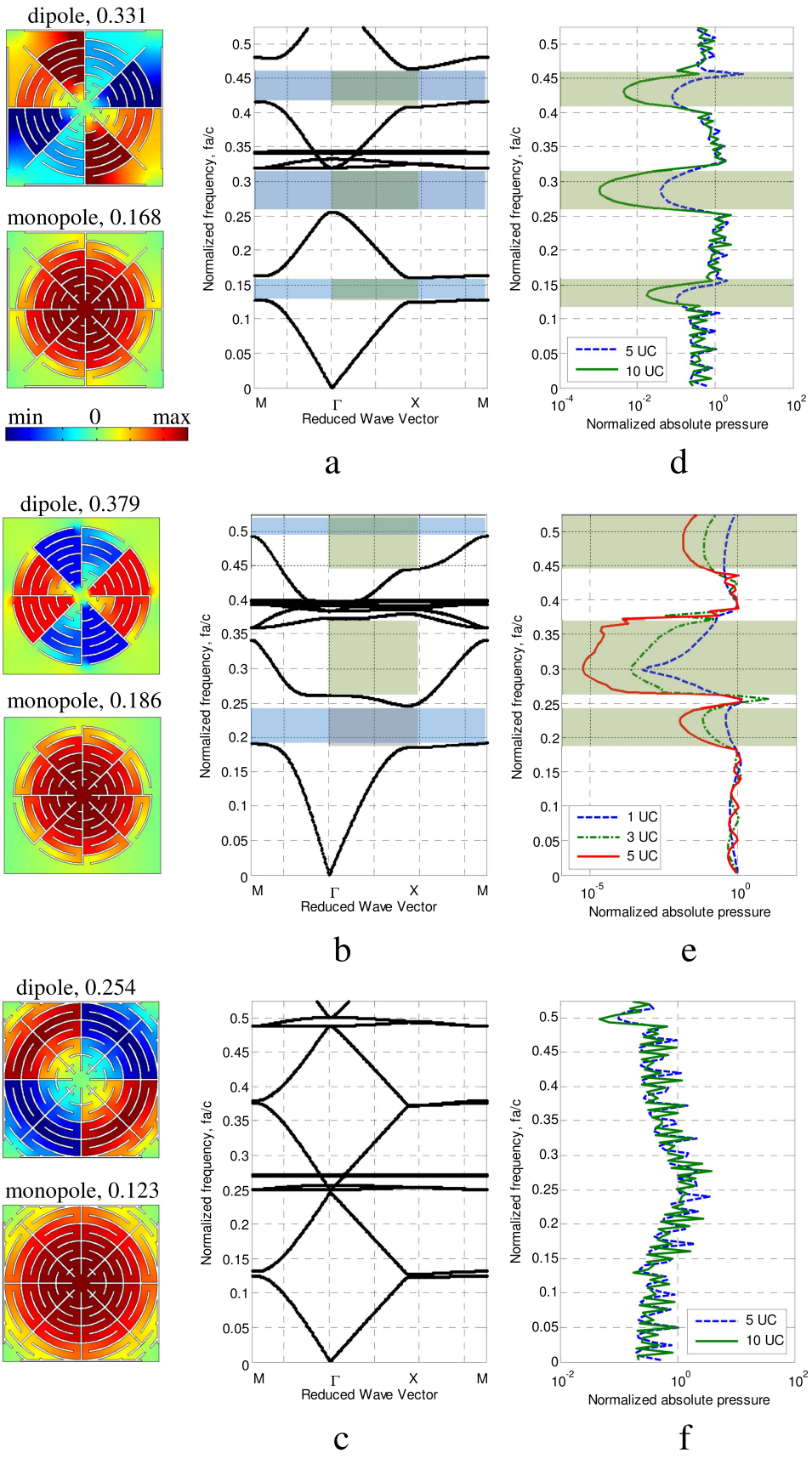

Figure 3. Dispersion and transmission spectra for a spider web-structured LAMM (a), (d), for a LAMM without square frame (b), (e) and for a spider web-structured LAMM with filled cavities (c), (f). The insets on the left indicate the normalized frequencies and pressure distributions for the artificial monopole and dipole Mie resonances. Omnidirectional band gaps are shaded in blue, while partial band gaps for the ΓX direction are depicted in green. The legends for the transmission spectra indicate the number of unit cells used in the model.

$\Omega = \omega a/2\pi c = fa/c$. The distinctive characteristics of the spectrum are the presence of bands with negative group velocity, three subwavelength band gaps and several flat bands with near-zero group velocity.

Note that in this work we focus on the subwavelength frequency range, so that the maximum value of the considered frequencies is restricted to $\Omega = 0.525$ ($f = 200$ Hz) that corresponds to the case when the wavelength is about twice the unit cell pitch ($f_{\max} a/c_{\text{air}} = a/\lambda_{\min} = 0.5$). Since at band-gap frequencies and for negative group velocity modes, the wavelengths are around five times larger the external unit cell dimensions (figures 3(a), (b)), here we speak of the deep sub-wavelength performance of the designed metastructure.

Figures 3(b) and (c) show dispersion diagrams for a LAMM unit cell without an external square frame and a spider web-structured LAMM with filled cavities, respectively. The dispersion spectrum for the first case (figure 3(b)) exhibits low-frequency band gaps, and in general, is similar to that for out-of-plane shear waves in locally resonant acoustic metamaterials [20]. For the spider-web structured LAMM with filled cavities, the spectrum has a conical-type structure formed by bands, which are separated by negligible band gaps and have negative group velocity at certain frequencies (figure 3(c)). In this case, the wave dispersion resembles that of zig-zag labyrinthine metamaterials with folded channels [7, 8, 10, 14].

When comparing figures 3(b) and (c) with figure 3(a), it becomes apparent that the spider-web structured LAMM has hybrid dispersion characteristics combining those of the two other LAMM structures. In particular, the designed configuration exhibits low-frequency band gaps similar to the LAMM without a square frame, and simultaneously has modes with a negative group velocity, such as those in the spectrum of LAMMs with folded channels [7].

Note that for the same geometric parameters of the unit cells, the band gaps for the spider web-structured LAMM (figure 3(a)) are located at about 1.5 times lower frequencies compared to those of the LAMM without the frame (figure 3(b)). Thus, due to the scalability of dispersion properties, unit cells with $a = 0.09$ cm should allow the manipulation of waves with frequencies down to 400–600 Hz, while maintaining a much lower total weight relative to most locally resonant structures [2, 20]. Also, by varying the size of the edge cavities, the band gaps can be shifted in frequency or even completely closed, when the cavities are filled by curved channels (such as in figure 3(c)).

The dispersion spectra in figures 3(a) and (c) exhibit several localized modes, which are characterized by pressure distributions similar to artificial Mie monopole and multipole resonances originally found for metastructures without a square frame [11]. The corresponding mode shapes are shown as insets in the spectra in figure 3. It is well-known that monopole Mie resonances are directly related to negative values of an effective bulk modulus, which occur at frequencies above this mode [21]. For the LAMMs with and without the square frame, the normalized frequencies of the monopole Mie resonance are 0.168 and 0.186, forming a lower and upper bound of the first (lowest) band gap, respectively. The dipole Mie resonance is commonly associated with negative effective mass density occurring below the resonance frequency [21]. In figures 3(a) and (b), this mode is found at $fa/c = 0.331$ and 0.379, respectively, i.e. the upper bound of the second band gaps. If frequency ranges with negative values of an effective bulk modulus and effective mass density are overlapped, double-negativity phenomena can be achieved [8, 9], the analysis of which is beyond the scope of this paper.

For the LAMM with filled cavities, pressure distributions at normalized frequencies 0.123 and 0.254 also resemble those for artificial monopole and dipole resonances. However, the band gaps around these frequencies are of negligible size. A possible reason for this is insufficient pressure localization within the unit cell compared to the affected area of the sound field. The wave energy appears to be insufficiently trapped, i.e. almost equally distributed within the unit cell, and is thus allowed to propagate.

3.2. Transmission analysis

The spectra in figures 3(d)–(f) show the magnitude of normalized absolute pressure, $\log \int_A |p_{\text{tr}}/p_{\text{in}}|\ \mathrm{d}A$ (with subscripts indicating transmitted and incident pressure, and A designating the area of a single unit cell), versus the normalized frequency fa/c. High transmission losses are found at the band gap frequencies predicted by the dispersion analysis. The slight discrepancies are attributed to the finite size of the model for the transmission simulations. Clearly, the magnitude of the transmission reduction depends on the number of the involved unit cells. For example, five unit cells of the LAMM without a square frame ensure significant transmission losses within the second band gap (figure 3(e)), while the same number of unit cells of the spider web-structured LAMM (figure 3(d)) provide less efficient attenuation, by about 3 orders of magnitude. This can be due to lower pressure localization in the presence of the frame, which restricts the affected volume of sound. Transmission losses can be enhanced by increasing the number of the unit cells in the model, as shown in figure 3(d). Taking this into account, a practical compact-size configuration of LAMMs can be achieved by stacking unit cells one on top of the other [10].

The spectrum for the LAMM with filled cavities in figure 3(f) indicates almost uniform frequency-independent transmission within the analyzed range regardless of the number of involved unit cells. This behavior is typical for the zig-zag labyrinthine metamaterials [7, 10]. Multiple small-magnitude transmission

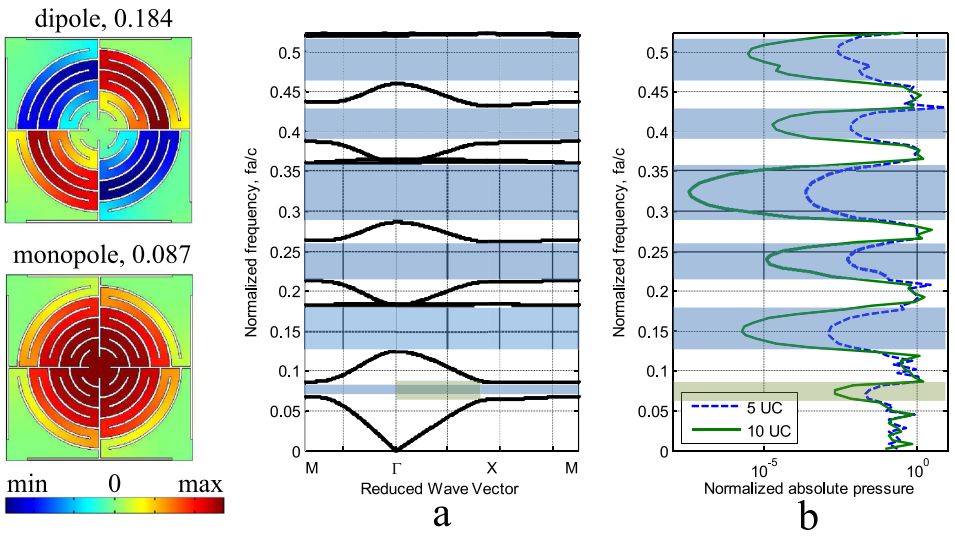

Figure 4. Dispersion (a) and transmission (b) spectra for a spider web-structured LAMM with four sectorial channels connected at the center. The insets on the left indicate the normalized frequencies and pressure distributions for the artificial monopole and dipole Mie resonances. Omnidirectional band gaps are shaded in blue, while partial band gaps for the ΓX direction are depicted in green. The legend for the transmission spectrum indicates the number of unit cells used in the model.

dips in figure 3(f) and similar dips below the first band gap in figure 3(d) correspond to zero pressure points at the nodes. For example, the dip around $f = 5$ Hz in figure 3(d) appears at the first spatial node of a mode with a wavelength $\lambda = c/f = 68.60$ m. This node is located at $\lambda/4 = 17.15$ m, i.e. approximately the distance from the wave source to the acquisition point through five unit cells of the metamaterial (for a single unit cell, $\eta a\sqrt{2} \approx 3$ m) and three homogeneous air unit cells (2.7 m long) also present in the model.

Finally, we note that the hybrid features of the spider web-structured LAMMs are also found for a four-channel configuration, the dispersion and transmission characteristics of which are given in figure 4. As this configuration has a higher curling number (which defines how many times the sound waves circulate in a curved channel [11]), the band gaps are shifted to twice lower frequencies (compared to those in figure 3(a)). At the same time, frequency regions with negative group velocity are reduced.

3.3. Tunability of Mie resonances and band gap frequencies

For the LAMMs with and without a square frame, the artificial Mie resonances determine the location of subwavelength band gaps, as discussed above. Hence, by modifying their frequencies, one can tune the band gap frequencies to desired ranges. Reference [11] suggests an approach to tune the Mie-type resonances by changing the size and refractive index of the unit cell. In this work, we develop an alternative technique, based on introducing variability in the channel width.

The considered types of non-uniformities are inspired by the architecture of natural spider webs [16, 22]. Figure 5(a) shows a pattern of a typical spider web built by a garden spider (*Araneus diadematus*). One can observe non-equal distances between circumferential elements and missing links (defects) in the circumferential silks, thus forming an 'imperfect' architecture. We introduce some of these irregularities into the developed spider web-structured LAMM geometry to analyze their effects on the metamaterial functionalities.

Figures 5(b)–(e) present several modifications of the original spider web-structured unit cells. Figure 5(b) shows an 8-channel unit cell from which a curved wall of radius r_6 has been removed. This results in the formation of an internal cavity between the curved parts of the channel and variations in the coiling coefficient and the effective refractive index values of the LAMM.

In terms of dispersion characteristics, the presence of the cavity leads to a shift the first band gap to higher frequencies and the closing of the second and third band gaps (the corresponding diagram is not shown). Instead of these band gaps, two dispersion cones are formed similar to those in figure 3(c). The frequency of the monopole is shifted from 0.168 to 0.194 (+16%), while the dipole resonance remains unchanged. From a physical point of view, the disappearance of the band gaps can be attributed to a detrimental effect of the introduced internal cavity on the vibration localization at the multipole Mie resonances. This effect also leads to an increase in the monopole resonance frequency, since a conventional LAMM of smaller length supports eigenmodes of smaller wavelength. If the cavity is located between the walls of radii r_4 and r_6, the dispersion spectrum (not shown) has two band gaps between 0.144 and 0.173, 0.412 and 0.543 with monopole and dipole Mie resonances at 0.173 and 0.320, respectively. Thus, the second band gap is closed for the same reason as in the

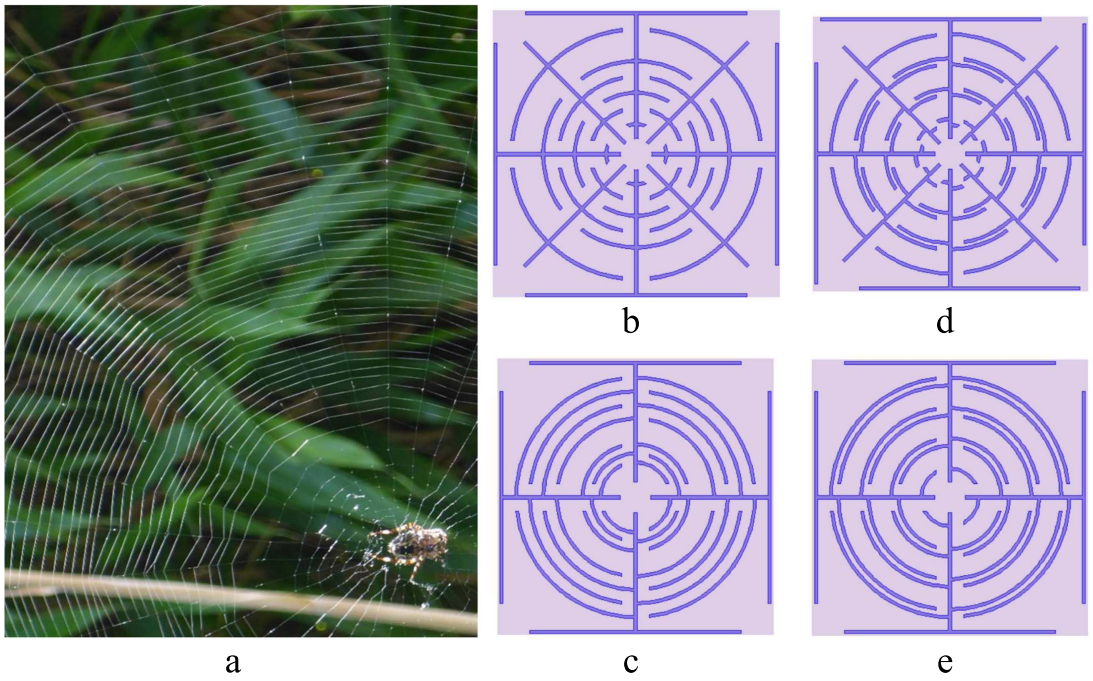

Figure 5. (a) Spider web woven by a garden spider Araneus diadematus (photo by D Krushinsky) (b) unit cell of a spider web-structured LAMM with a cavity inside the sectorial channels formed by removing one of the solid walls from the initial geometry shown in Figure 1(a). (c) Unit cell with a cavity and two areas with curved channels of different width. This configuration resembles the architecture of the spider web in (a) and additionally allows to preserve approximately the same coiling coefficient as in figure 1(b). (d), (e) Unit cells with a periodically varying width of the curved channels.

Table 1. External radii r_i ($i = 1, \ldots, 7$) of solid walls for the spider web-structured LAMM unit cells with eight sectorial channels shown in figure 5(c).

	r_1	r_2	r_3	r_4	r_5	r_6	r_7
Case 1	0.12a	0.15a	0.18a	0.265a	0.31a	0.355a	0.4a
Case 2	0.12a	0.14a	0.16a	0.25a	0.3a	0.35a	0.4a
Case 3	0.12a	0.14a	0.16a	0.295a	0.33a	0.365a	0.4a

previous case. On the contrary, the absence of any wall of radius r_i with $i = 1$–4 does not significantly affect the dispersion properties of the LAMM: the dispersion bands (not shown) have similar trends as those in figure 3(a), the three band gaps are preserved, and the frequencies of the Mie resonances are only slightly shifted from the values for the regular unit cell configuration (figure 1(a)). Therefore, the incorporation of a cavity within the sectorial channels by eliminating a large-radius curved wall enables to reduce the highly reflective properties of the unit cell attributed to multipole Mie resonances, and to simultaneously introduce conical dispersion by preserving the first subwavelength band gap governed by the monopole resonance.

Figure 5(c) shows another example of the incorporation of an internal cavity between curved channels by separating two channel parts, while reducing their width. Note that the designed configuration closely replicates the architecture of a spider web shown in figure 5(a). The values of the circular channel radii for the analyzed metastructures are indicated in table 1. In all the considered cases, the cavity is located closer to the unit cell center, between the walls of radii r_3 and r_4.

First, we consider 'Case 1' in which the width of the channel part external (or internal) to the cavity equals 0.045a (or 0.03a). These parameters allow to approximately preserve the coiling coefficient equal to that of the regular configuration (figure 1(a)). The dispersion diagram for Case 1 (not shown) is the same as the one in figure 3(a) (the reference) up to the normalized frequency 0.210. At higher frequencies, most of the bands are shifted to lower frequencies as compared to the reference case, with a shift in the dipole resonance frequency from 0.331 (for the regular unit cell) to 0.311 (−6% shift). The size of the second band gap is almost unchanged, while the third band gap is increased by about 1.5 times. Next, we consider 'Case 2', in which the channel part external to the cavity has the same width as the regular configuration, i.e. 0.05a, and the internal part a smaller width (0.02a). The dispersion diagram is again similar to the reference with bands shifted to lower or higher frequencies. In particular, the first band gap is twice smaller, as the lowest band is shifted to higher frequencies,

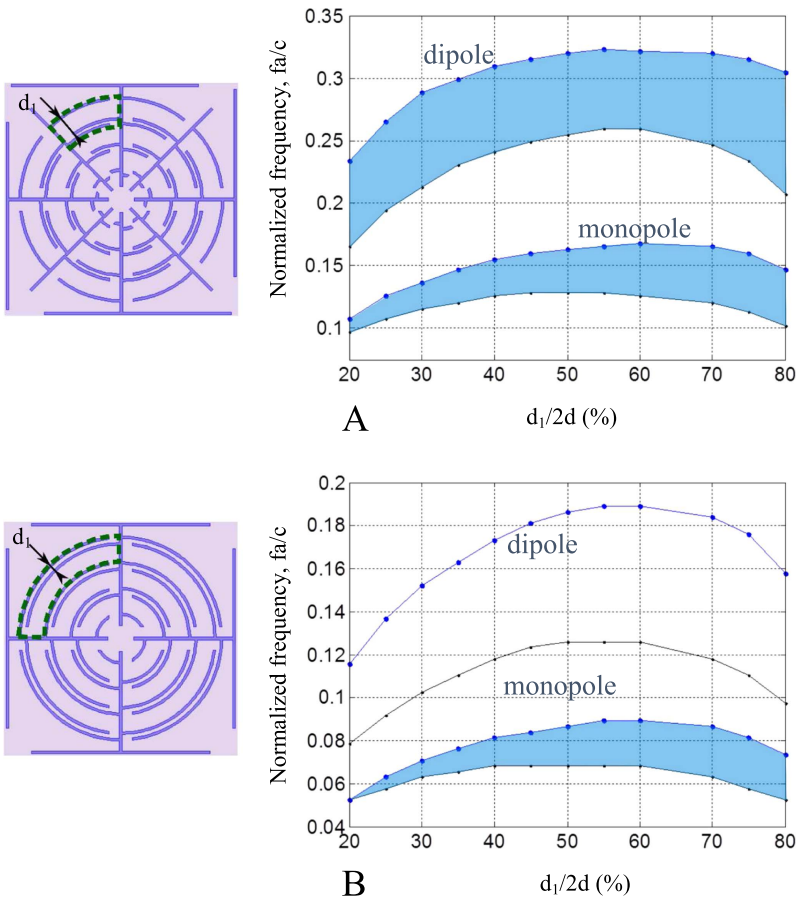

Figure 6. Variation of the band gap frequencies (shaded in blue) and monopole and dipole Mie resonances for unit cells with a periodically varying width comprising (a) eight and (b) four curved channels.

though the monopole frequency is unchanged. The second bad gap almost disappears, since the dipole resonance is shifted down to a normalized frequency of 0.257. The third band gap (governed by the quadrupole Mie resonance) is enlarged and spans between the frequencies 0.346 and 0.460. If the cavity size is further increased by reducing the width of the channels in the external part to $0.035a$ ('Case 3'), the third band gap is further enlarged and becomes 3.7 times larger than that of the reference configuration. In this case, the monopole and dipole frequencies are at 0.129 and 0.231, respectively.

Thus, the presence of an internal cavity and different width of the channel parts do not significantly modify the structure of the dispersion diagrams, whereas the frequencies of band gaps and the Mie resonances can be efficiently tuned. In general, to obtain a non-negligible shift of the monopole frequency, it is necessary to introduce a large cavity. This is because the frequency of the monopole resonance is governed by external sizes r_1 and r_7 and appears to be insensitive to small changes in the coiling coefficient values [11]. In contrast to this, the dipole (and quadrupole) resonances can easily be tuned due to the presence of an internal cavity, and thus, the ranges of second and third band gap frequencies can be shifted. This occurs since the location of the vibration maxima in the corresponding mode shapes are sensitive to the channel architecture. In particular, a combination of a large cavity and thin curved channels (as in Case 3) enables the achievement of comparatively wide third band gap. This feature can be effectively exploited to design broadband low-frequency sound absorbers.

Finally, we consider unit cells with a periodically varying width of the curved channels, shown in figures 5(d), (e). These configurations are described by the following values of external radii: $r_i = 0.05(i + j) + 0.02$ for $i = 2,\ 4,\ 6$ and $j = 0,\ 1, \ldots, 8$. Figures 6(a), (b) show normalized frequencies of subwavelength band gaps and the monopole and dipole Mie resonances for the eight- and four-sectorial channel configurations, respectively, as a function of the parameter $d_1/2d$, where the d_1 dimension is schematically shown in the inset on the left. For a regular configuration (one with curved channels of constant width), $d_1/2d = 50\%$. It can be seen that the monopole and dipole resonances can be shifted up to 40% by exploiting a periodically varying channel width. Maximum variations occur for $d_1 < 50\%$. Again, as for the previously considered cases, the frequency of the monopole resonance varies less as compared to the dipole. The band gap frequencies vary as a function of the channel width. The first band gap is, in general, shifted to lower frequencies compared to the regular

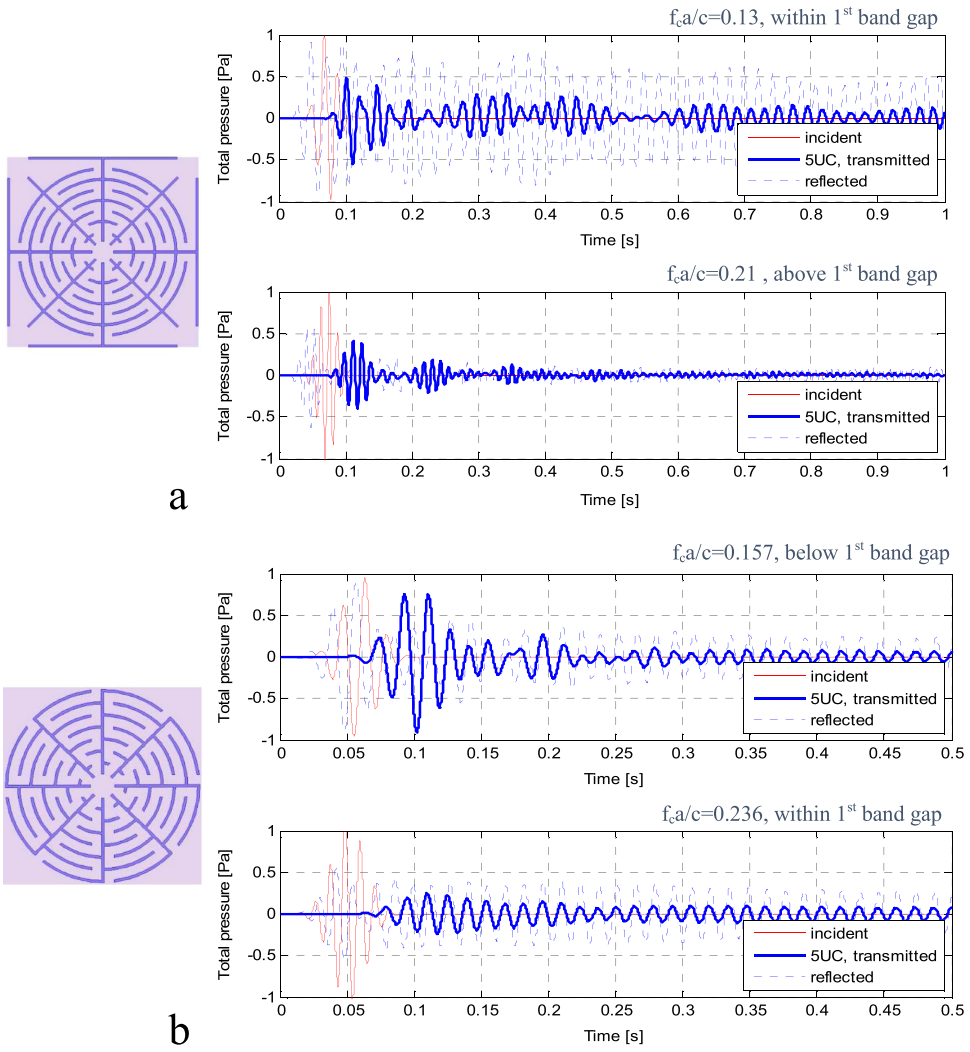

Figure 7. Transient analysis of a Gaussian modulated sinusoidal pulse with the central frequency f_c propagating though a set of 5 closely-located unit cells (shown in red). The presence of edge cavities (a) enables better wave reflection performance on band gap frequencies (governed by the monopole Mie resonance) compared to the metastructure without edge cavities (b).

configurations, and can even be closed, when $d_1/2d \approx 20\%$. The second band gap also tends to lower frequencies and becomes wider for $d_1/2d \geqslant 60\%$. Thus, the exploitation of a periodically varying channel width enables to access a challenging low-frequency range while preserving external structural sizes.

3.4. Transient analysis

Finally, to evaluate the effectiveness of the proposed metastructures for manipulating low-frequency sound and the advantages of introducing a surrounding frame, we have performed transient simulations in the time domain. Figure 7 shows calculated transmitted (solid blue line) and reflected (dashed blue line) signals for the LAMMs with and without the square frame composed of five unit cells. The reflected part of signal is estimated at a point beyond the metamaterial structure at a distance $a/2$ and, thus, also includes the incident part. Incident pulses of different carrier frequencies f_c are indicated in red. They are calculated for the reference configuration, in which the metamaterial region is removed. The absence of reflected waves in the latter case proves the reliability of the implemented radiation condition at the right boundary.

As expected, for every carrier frequency, the signal transmitted through the metamaterial is shifted to a later time, due to the lower effective sound propagation velocity in the structure. Also, the signals are substantially attenuated. The level of attenuation depends on the carrier frequency and ranges from 25% to 50% for frequencies outside the band gaps and from 60% to 70% within the band gaps. Since viscoelastic losses are not accounted for in the model, this means that a pulse is 'trapped' by the metamaterial structure. After multiple reflections, its energy is gradually released and appears as tail pulses to the initial transmitted pulse.

Outside the band gaps, the signal preserves its shape and is followed by a series of self-repeating patterns of a gradually decreasing amplitude. The small magnitude of the reflected waves in the lower subfigure of figure 7(a)

proves that most of the incoming energy is transmitted as several pulses of smaller amplitude and separated in time.

Within the band gaps, on the contrary, the transmitted signal does not preserve its shape due to the peculiar dynamics of the monopole Mie resonance governing the band gap generation mechanism [11]. The influence of this resonance can clearly be seen by analyzing the reflected signals. For the LAMM without a frame (figure 7(b)), the magnitude of the reflected signal in the band gap is comparable to that for the pulse with the carrier frequency outside the band gap. For the spider web-structured LAMM (figure 7(a)), instead, the reflected signal is much stronger, indicating improved reflectivity achieved due to the presence of the external frame.

4. Conclusions

In this paper, we have developed a new type of LAMMs with hybrid sound-wave manipulation characteristics, drawing inspiration from the architecture of natural spider webs. The developed metastructures are characterized by the simultaneous presence of band gaps at deep subwavelength scales, which are governed by the artificial Mie resonances, and bands with a negative slope tending to produce conical dispersion. This is achieved by adding a surrounding square frame to sectorial circular-shaped channel configuration. An additional advantage of this design is the tunability of wave manipulation performance, i.e. switching on/off subwavelength band gaps and negative group-velocity frequencies by varying the unit cell organization, e.g. the number and width of the curved channels, as well as by introducing cavities externally at the unit cell corners or internally by diving the channels into two separate parts. The effects of variability in the channel width on the dispersion characteristics have been thoroughly analyzed. In particular, we find that the irregularities typical for the architecture of natural spider webs enable the tuning of the Mie resonances to lower frequencies and the extension of the band gap size up to almost four times while preserving structural dimensions. Additionally, we have demonstrated that the proposed trivial structural modification of adding the square frame allows the enhancing of the metamaterial functionality by changing its dynamics within and outside the band gaps. At the band gap frequencies, the highly reflective performance governed by Mie resonances is shown to improve with the interplay of the dynamics of the sectorial channels with that of the square frame. These findings can be useful for applications related to airborne sound/noise reduction with flexible and wideband tunability of the operating frequency ranges in the entire spectrum of low-frequency sound.

Acknowledgments

AOK has received funding from the European Union's 7th Framework programme for research and innovation under the Marie Skłodowska-Curie Grant Agreement No. 609402-2020 researchers: Train to Move (T2M). M M has received funding from the European Union's Horizon 2020 research and innovation programme under the Marie Skłodowska-Curie Grant Agreement No. 658483. NMP is supported by the European Research Council PoC grant 2015 SILKENE No. 693670, EU FETPROACTIVE grant 732344 'NEUROFIBRES', and by the European Commission under the Graphene Flagship (WP14 'Polymer Nanocomposites', No. 604391). FB is supported EU FETPROACTIVE grant 732344 'NEUROFIBRES'. Photo credit: Dr Dmitry Krushinsky.

ORCID iDs

A O Krushynska https://orcid.org/0000-0003-3259-2592
F Bosia https://orcid.org/0000-0002-2886-4519
M Miniaci https://orcid.org/0000-0002-6830-3548
N M Pugno https://orcid.org/0000-0003-2136-2396

References

[1] Deymier P A ed 2013 *Acoustic Metamaterials and Phononic Crystals* (*Springer Series in Solid-State Sciences*) (Berlin: Springer)
[2] Liu Z, Zhang X, Mao Y, Zhu Y, Yang Z, Chan C and Sheng P 2000 Locally resonant sonic materials *Science* **289** 1734
[3] Movchan A and Guenneau S 2004 Split-ring resonators and localized modes *Phys. Rev.* B **70** 125116
[4] Torrent D and Sanchez-Dehesa J 2009 Radial wave crystals: radially periodic structures from anisotropic metamaterials for engineering acoustic or electromagnetic waves *Phys. Rev. Lett.* **103** 064301
[5] Farhat M, Enoch S, Guenneau S and Movchan A 2008 Broadband cylindrical acoustic cloak for linear surface waves in a fluid *Phys. Rev. Lett.* **101** 134501
[6] Chen H, Chan C and Sheng P 2010 Transformation optics and metamaterials *Nat. Mater.* **9** 387–96
[7] Liang Z and Li J 2012 Extreme acoustic metamaterial by coiling up space *Phys. Rev. Lett.* **108** 114301

[8] Liang Z, Feng T, Lok S, Liu F, Ng K, Chan C, Wang J, Han S, Lee S and Li J 2013 Space-coiling metamaterials with double negativity and conical dispersion *Sci. Rep.* **3** 1614
[9] Xie Y, Popa B-I, Zigoneanu L and Cummer S 2013 Measurement of a broadband negative index with space-coiling acoustic metamaterials *Phys. Rev. Lett.* **110** 175501
[10] Frenzel T, Brehm J, Bueckmmann T, Schitty R, Kadic M and Wegener M 2013 Three-dimensional labyrinthine acoustic metamaterials *Appl. Phys. Lett.* **103** 061907
[11] Cheng Y, Zhou C, Yuan B, Wu D, Wei Q and Liu X 2015 Ultra-sparse metasurface for high reflection of low-frequency sound based on artificial Mie resonances *Nat. Mater.* **14** 1013–9
[12] Miniaci M, Krushynska A, Bosia F and Pugno N M 2016 Large scale mechanical metamaterials as seismic shields *New J. Phys.* **18** 083041
[13] Xie Y, Konneker A, Popa B-I and Cummer S 2013 Tapered labyrinthine acoustic metamaterials for broadband impedance matching *Appl. Phys. Lett.* **103** 201906
[14] Li Y, Jiang X, Li R, Liang B, Zou X, Yin L and Cheng J 2014 Experimental realization of full control of reflected waves with subwavelength acoustic metasurfaces *Phys. Rev. Appl.* **2** 064002
[15] Ko F and Jovicic J 2004 Modeling of mechanical properties and structural design of spider web *Biomacromolecules* **5** 780–5
[16] Cranford S, Tarakanova A, Pugno N and Buehler M 2012 Nonlinear material behaviour of spider silk yields robust webs *Nature* **482** 72–6
[17] Meyer A, Pugno N and Cranford S 2014 Compliant threads maximize spider silk connection strength and toughness *J. R. Soc. Interface* **11** 20140561
[18] Zaera R, Soler A and Teus J 2014 Uncovering changes in spider orb-web topology owing to aerodynamics effects *J. R. Soc. Interface* **11** 20140484
[19] Miniaci M, Krushynska A, Movchan A, Bosia F and Pugno N 2016 Spider web-inspired acoustic metamaterials *Appl. Phys. Lett.* **109** 071905
[20] Krushynska A, Kouznetsova V and Geers M 2014 Towards optimal design of locally resonant acoustic metamaterials *J. Mech. Phys. Solids* **71** 179–96
[21] Li J and Chan C 2004 Double-negative acoustic metamaterial *Phys. Rev.* E **70** 055602
[22] Aoyanagi Y and Okumura K 2010 Simple model for the mechanics of spider webs *Phys. Rev. Lett.* **104** 038102